Thin intergranular films and solid-state activated sintering in nickel-doped tungsten

Vivek K. Gupta [a], Dang-Hyok Yoon [a,1], Harry M. Meyer III [b], Jian Luo [a,c,*]

[a] *School of Materials Science and Engineering, Clemson University, Clemson, SC 29634, USA*
[b] *High Temperature Materials Laboratory, Oak Ridge National Laboratory, Oak Ridge, TN 37831, USA*
[c] *Center for Optical Materials Science and Engineering Technologies, Clemson University, Clemson, SC 29634, USA*

Abstract

Nickel-doped tungsten specimens were prepared with high purity chemicals and sintered. Although activated sintering starts more than 400 °C below the bulk eutectic temperature, the nickel-rich crystalline secondary phase does not wet the tungsten grain boundaries in the solid state. These results contrast with the classical activated sintering model whereby the secondary crystalline phase was presumed to wet grain boundaries completely. High resolution transmission electron microscopy and Auger electron spectroscopy revealed the presence of nanometer-thick, nickel-enriched, disordered films at grain boundaries well below the bulk eutectic temperature. These interfacial films can be regarded as metallic counterparts to widely observed equilibrium-thickness intergranular films in ceramics. Assuming they form at a true thermodynamic equilibrium, these films can alternatively be understood as a class of combined grain boundary disordering and adsorption structures resulting from coupled premelting and prewetting transitions. It is concluded that enhanced diffusion in these thin intergranular films is responsible for solid-state activated sintering.
© 2007 Acta Materialia Inc. Published by Elsevier Ltd. All rights reserved.

Keywords: Sintering; Grain boundary wetting; Grain boundary diffusion; Interface segregation; Refractory metals

1. Introduction

Solid-state activated sintering refers to the enhancement of densification caused by minor solid-state additives. A well-known example is the accelerated sintering of tungsten and other refractory metals (Mo, Nb and Ta) resulting from the addition of less than 0.5 wt.% of transition metals (e.g., Ni, Pd, Co, Fe and Pt), which can initiate below 60% of the corresponding bulk solidus or eutectic temperatures [1–15]. Since densification occurs at low temperatures where bulk diffusion is usually insignificant, grain boundary (GB) transport is generally implicated. In a phenome-

nological model extended from liquid-phase sintering theory [16], solid-state activated sintering was attributed to the enhanced mass transport of the base material in an "activator" phase [1]. An effective solid-state activator should have high solubility and transport rate for the base material and should remain segregated at GBs.

In principle, the solid-state activators can be (i) crystalline secondary bulk phases that penetrate along the GBs, (ii) Langmuir–McLean or truncated BET (Brunauer–Emmett–Teller) type interfacial segregation/adsorption region without precipitation of a discrete phase or (iii) discrete nanoscale interfacial phases that do not appear in bulk phase diagrams. Although the phenomenon of solid-state activated sintering has been studied over five decades [1–15,17,18], the exact nature of these solid-state activators and how they result in enhanced sintering remain largely unknown.

Solid-state activated sintering has also been observed in several ceramic systems [19–22]. A previous study [19]

---

* Corresponding author. Address: School of Materials Science and Engineering, Clemson University, Clemson, SC 29634, USA.
 E-mail addresses: jianluo@clemson.edu, jluo@alum.mit.edu (J. Luo).
[1] Present address: School of Materials Science and Engineering, Yeungnam University, Korea.

using Bi_2O_3-doped ZnO as a model ceramic system found that approximately 1-nm thick amorphous films form at GBs and on some free surfaces well below the bulk eutectic temperature, concurrently with the onset of accelerated sintering. Consequently, activated sintering in this system was attributed to accelerated mass transport through these sub-eutectic, disordered, interfacial films. These nanoscale intergranular [23,24] and surficial [25–28] films are "quasi-liquid" layers that are stabilized at interfaces below the bulk eutectic temperature, where phenomenological similarities to the theories of premelting [29–32] and prewetting [33] exist. Recently, a similar solid-state activated sintering mechanism caused by disordered GBs has been inferred for another ceramic system [34,35].

Nickel-doped tungsten has been widely studied as a model refractory metal system for activated sintering [1,2,4,5,7–9,14]. In a classical model [1], the solid-state activator is presumed to be the secondary, crystalline, Ni-rich phase which completely "wets" the tungsten primary phase and penetrates along the GBs. However, the occurrence of solid-state GB wetting has not been confirmed.

On the other hand, the Ni-doped W system [1,2,4,5,7–9,14] exhibits activated sintering and other characteristic behaviors that are similar to Bi_2O_3-doped ZnO [19]. In sintered specimens, nickel was found to segregate at tungsten GBs [4,36,37]. Radiotracer experiments indicated that <1 at.% nickel addition can result in about a 10^3 times increase in tungsten GB diffusivities and the existence of a discontinuity in the Arrhenius plot of diffusivities [38], suggesting the possible occurrence of a GB structural transition. Previous sintering experiments [4,9,10] also showed that the optimal doping level is about the equivalence of ~1 nm Ni coating on initial W particles and further addition beyond the optimal level does not generate additional benefits. These observations suggest that enhanced sintering occurs in a nanoscale interfacial phase for Ni-doped W, akin to that observed for Bi_2O_3-doped ZnO [19]. Furthermore, a recent study [14] suggested that the solid-state activated sintering of W is due to a GB roughening transition induced by Ni segregation, where the atomic level GB structures have not been characterized. In a recent letter [39], we reported the stabilization of nanometer-thick, quasi-liquid GB layers in Ni-doped W well below the bulk eutectic temperature. This study is motivated by the critical need to investigate wetting and segregation behaviors in Ni-doped W and to reveal the mysterious solid-state activated sintering mechanism in refractory metals.

2. Experimental procedure

High purity tungsten powder (99.999%) with an average size of 4–6 μm was purchased from Alfa Aesar (Ward Hill, MA). To obtain a uniform nickel distribution, nickel chloride ($NiCl_2 \cdot 6H_2O$, 99.9998%, Alfa Aesar) was dissolved in methanol and mixed with the tungsten powder. The mixture was first dried at 80 °C for 20 min and then calcined in a tube furnace flowing N_2 + 5% H_2 at 600 °C for 1 h.

The calcined powder was compacted without any binder at approximately 80 MPa into cylindrical pellets of 6 mm diameter and 4–5 mm thickness. The green pellets were sintered isothermally in a tube furnace flowing N_2 + 5% H_2 for 2 h and cooled with the furnace shut down. The cooling rate was measured to be ~30 °C/min at 1400 °C.

The first set of specimens were doped with 0.05, 0.1, 0.2, 0.3, 0.5 and 1.0 at.% nickel, respectively, and sintered at 1400 °C for 2 h. The second set of specimens were doped with 1.0 at.% nickel and sintered at 1100 °C, 1150 °C, 1200 °C, 1250 °C, 1300 °C, 1350 °C, 1400 °C, 1450 °C and 1475 °C, respectively, for 2 h. Additionally, a tungsten specimen containing 20 at.% nickel was sintered at 1400 °C for 2 h for a solid-state wetting experiment. All specimens were sintered in solid-state well below the bulk eutectic temperature of 1495 °C (Fig. 1) [40]. In order to probe the solid-state densification mechanism and avoid the effects of final stage grain growth, we kept the final densities below 90% of the theoretical density. Thus, these experiments represent the initial and intermediate stages of sintering.

The sintered specimens were examined by scanning electron microscopy (SEM, Hitachi S3500 and S4700) equipped with energy dispersive X-ray analysis (EDX) detectors. Specimens were either fractured or cut and polished. The polished specimens were etched with HNO_3:3HCl (boiling) or H_2O_2 (hot) solutions. Grain sizes were measured by standard interception methods and the average intercept lengths were recorded. The green and sintered densities were calculated based on measured weight and dimensions.

Auger electron spectroscopy (AES) was conducted to measure the GB chemistry. A special fixture was designed to fracture the specimens in situ in the ultra high vacuum (UHV) chamber of the scanning Auger microscope (SAM, PHI 680). Since these specimens typically undergo a brittle intergranular failure caused by GB embrittlement; the fractured surfaces represent GBs. The specimens were sputtered with an argon ion beam to obtain depth profiles. Three spots were randomly selected for Auger analysis; means and standard deviations were reported. The amount of carbon and oxygen was monitored by Auger spectroscopy. In cases of substantial carbon contamination, which occurred only occasionally (presumably, it is related to the
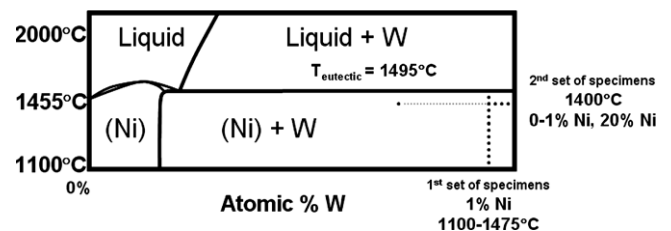

Fig. 1. W–Ni phase diagram between 1100 °C and 2000 °C [40], in which the positions of the specimens used in the study are schematically illustrated. Several intermediate compounds form below 1060 °C, but crystalline Ni and W are the only stable bulk phases between 1060 °C and 1455 °C. The solid solubility limit of Ni in W is approximately 0.3 at.% at the eutectic temperature 1495 °C and ~0.2 at.% at 1400 °C.

adsorption and the release of the lubrication fluid, which was used in cutting specimens for Auger analysis, from the pores in these specimens), new specimens or spots were selected for re-testing. Self-supported discs of 3-mm diameter were cut for preparing transmission electron microscopy (TEM) specimens. These specimens were pre-thinned by a standard polishing and dimpling procedure, followed by ion milling. Low incident angles were used to minimize milling damage. High resolution transmission electron microscopy (HRTEM) was conducted using a 400 keV microscope (JEOL 4000EX).

3. Results

3.1. Densification and microstructure

The average green density is about 67–68% of the theoretical value. The relative density and grain size versus

nickel dopant content for specimens sintered at 1400 °C is shown in Fig. 2a, wherein each data point is an average of three or more specimens. In this set of specimens, ∼1% densification is observed for the pure tungsten specimen while more than 20% densification (to ∼89% of the theoretical density) is achieved for specimens containing 0.5–1.0 at.% nickel. The densification rate increases monotonically with increasing dopant percentage for specimens containing less than 0.2 at.% Ni, and approaches a plateau for specimens doped with 0.3 at.% or more Ni. A similar trend is also observed for grain growth. The average intercept length increases with the Ni content, from ∼2 μm for specimens containing 0.05 at.% Ni to ∼10 μm for those containing 0.3 at.% Ni. The grain size shows little variation for specimens doped with 0.3–1.0 at.% Ni. The difference in porosity for pure and doped specimens is clearly seen in SEM micrographs (Fig. 3a and b). Substantial neck and grain growth is also evident in the Ni-doped W specimens (Fig. 3b).
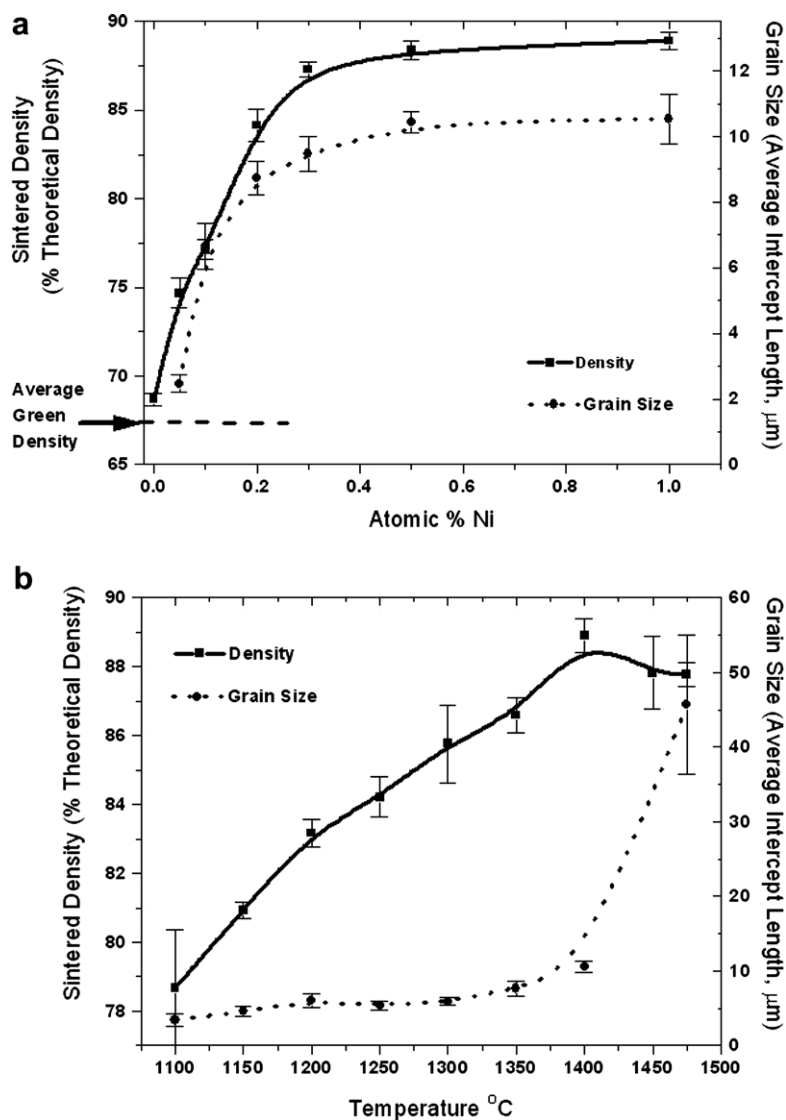

Fig. 2. (a) Relative density (solid line) and grain size (dotted line) versus nickel content for specimens sintered at 1400 °C for 2 h. (b) Relative density and grain size versus sintering temperature for 1 at.% Ni specimens sintered isothermally at 1100–1475 °C for 2 h. Error bars represent standard deviations.
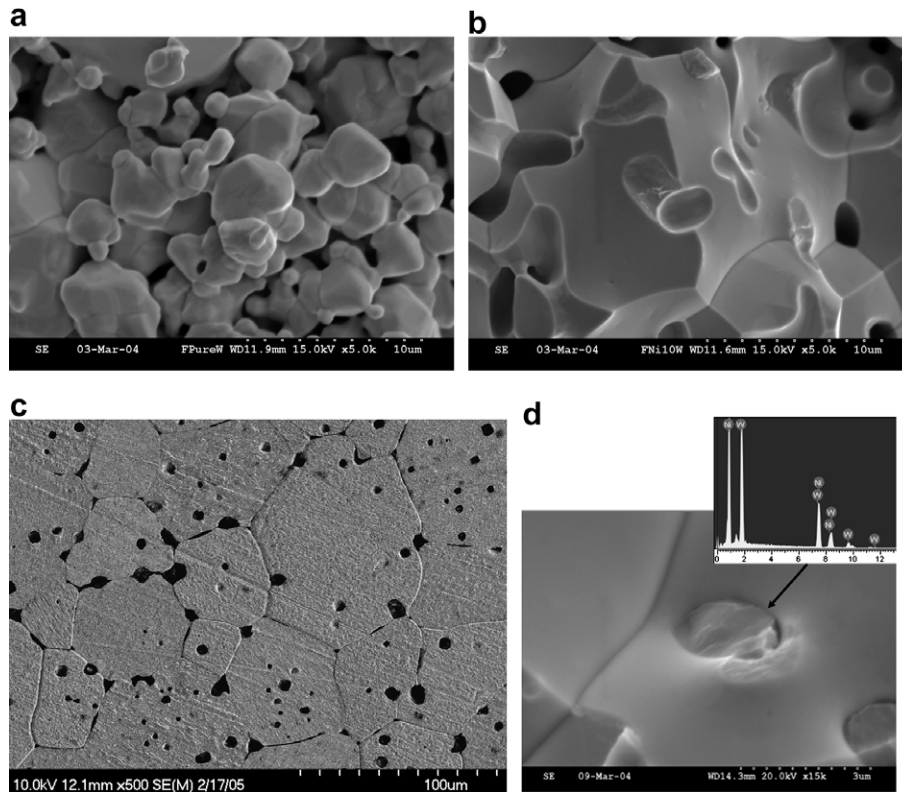
Fig. 3. SEM micrographs of (a) a pure W specimen sintered at 1400 °C, (b) a 1.0 at.% Ni-doped W specimens sintered at 1400 °C, and (c) and (d) 1.0 at.% Ni-doped W specimens sintered at 1475 °C. Pore-boundary separation and precipitate-boundary separation are seen in (c) and (d), respectively. The inset in (d) is an EDX spectrum indicating that the particle is the Ni-rich secondary phase. All specimens were sintered isothermally for 2 h. The specimens shown in (a), (b) and (d) were fractured and the specimen shown in (c) was cut, polished and etched.

The relative density and grain size versus sintering temperature for 1.0 at.% nickel doped specimens is shown in Fig. 2b. In this second set of specimens, which were sintered at 1100–1475 °C for 2 h, the relative density increases with increasing sintering temperature from ~79% at 1100 °C to ~89% at 1400 °C. However, the sintered density decreases slightly as the sintering temperature is further increased above 1400 °C. The grain size is virtually the same for the specimens sintered between 1100 °C and 1400 °C despite increasing density. Significant grain growth occurs at 1475 °C. The large grain size for specimens sintered at 1475 °C is clearly evident in the SEM micrograph shown in Fig. 3c. Furthermore, significant pore-boundary separation and precipitate-boundary separation are observed for specimens sintered at 1475 °C (Fig. 3c and d), indicating a high GB mobility. Some pore-boundary separation is also evident for specimens sintered at 1400 °C, but to a much lesser extent.

3.2. Solid-state wetting configuration

To identify the solid-state wetting configuration clearly, a model experiment has been performed with a tungsten specimen doped with 20 at.% nickel and sintered at 1400 °C for 2 h. The sintering density is ~96% of theoretical density for this specimen containing excess nickel. The secondary Ni-rich bulk phase does not wet and penetrate

along GBs (Fig. 4). The dark particles in Fig. 4 are the Ni-rich phase, which have been verified by EDX analysis. Quantitative EDX analysis shows that these secondary
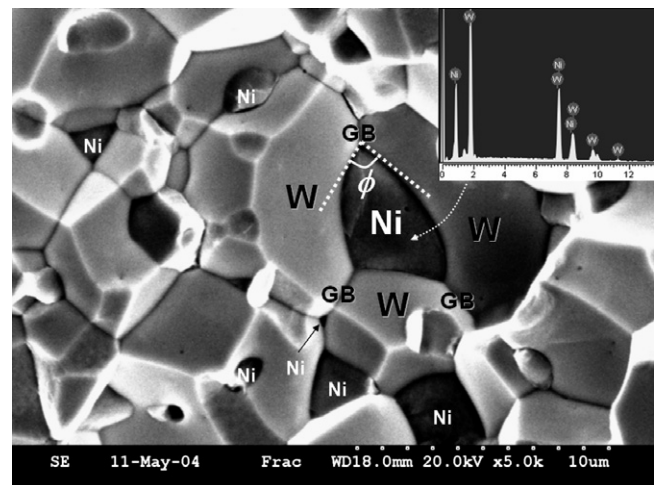

Fig. 4. SEM micrograph of a fractured surface of a W + 20 at.% Ni specimen sintered at 1400 °C for 2 h. The Ni-rich phase particles (labeled) have darker contrast. The inset is an EDX spectrum of a point analysis with a beam sitting on the Ni-rich phase particle; quantitative EDX analysis showed that the Ni content of these particles represents the equilibrium Ni-rich phase. The secondary nickel-rich phase does not completely wet GBs; otherwise the dihedral angle (ϕ) should be zero.
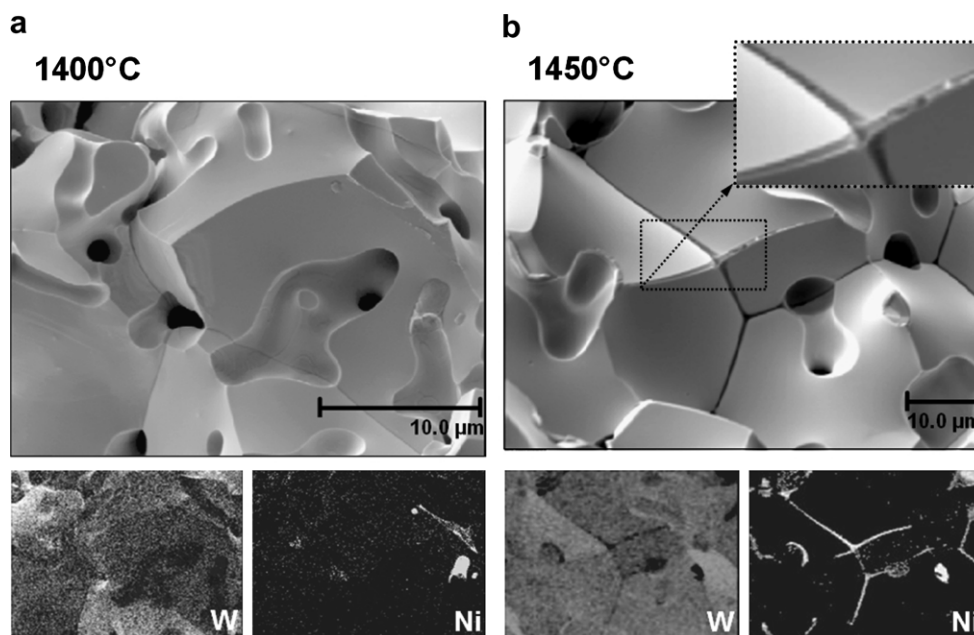
Fig. 5. SEM images and Auger W/Ni maps for fractured surfaces of specimens sintered at (a) 1400 °C and (b) 1450 °C respectively. Both specimens contain 1 at.% Ni and were sintered for 2 h. Auger compositional mapping was conducted after sputtering off the nanoscale segregation layers at fractured GBs. The Ni-rich secondary phase is present at triple junctions in (b) but not in (a). The inset in the top right corner of (b) shows the triple-grain and four-grain junctions in an expanded view.

phase contains ∼80 at.% Ni, which is consistent with the composition of the Ni-rich crystalline phase in the phase diagram (Fig. 1) [40] and indicates that a chemical equilibrium has been achieved in these specimens. The observed (apparent) dihedral angles (ϕ) projected on the fractured surface are as high at 70° in Fig. 4. The real dihedral angle (in the three-dimensional space) can be different and should be anisotropic, but it is reasonable to conclude that it must be significantly greater than zero. The Ni-rich secondary phase is typically present as isolated particles at four-grain junctions (i.e. they have four neighboring grains, even if only three neighboring grains are typically observed in SEM micrographs of fractured specimens).

Moreover, the Ni-rich secondary phase does not wet the triple-grain junctions at 1400 °C. This is evident from the SEM image in conjunction with high spatial resolution Auger compositional maps (Fig. 5a) of W + 1 at.% Ni specimens. To remove the effect of nanoscale Ni segregation at fractured GBs, these specimens were briefly sputtered with an argon beam before conducting the compositional mapping. When the temperature is increased to 1450 °C, the Ni-rich secondary phase wets triple-grain junctions (Fig. 5b), but it still does not wet GBs.

3.3. Grain boundary chemistry and structure

Ni/W ratios at fractured GBs were measured by Auger electron spectroscopy (AES). Depth profiling was conducted by measuring the AES signals while sputtering the fractured surfaces with an argon ion beam. A representative measured Ni/W ratio versus sputtering time is shown in Fig. 6. Nickel is clearly segregated at the fractured

GBs. The sputtering rate was calibrated to be 2 nm min^{-1} for a SiO_2 standard under the same sputtering conditions. While a different sputtering rate is expected for W–Ni, the thickness of the segregation layer is likely to be on the order of 1 nm. To quantify the relative thickness of the segregation layer better, the Ni/W ratio versus sputtering time ($X^{Ni/W}(t)$) was fitted with a generic exponentially decaying function:

$$X^{Ni/W}(t) = X_0^{Ni/W} \cdot \exp\left(-\frac{t}{\tau_s}\right) \qquad (1)$$

where τ_s is a parameter representing the "sputtering time" or the "relative thickness of the segregation layer".
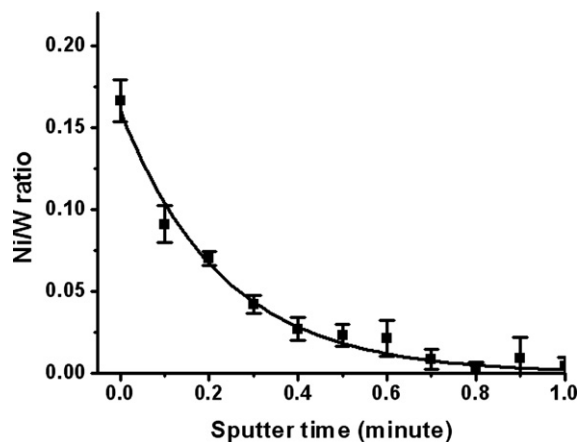

Fig. 6. Ni/W ratio versus sputter time for a W + 1.0 at.% Ni specimen sintered at 1400 °C for 2 h. Error bars represent standard deviations. The curve is fitted with an exponentially decaying function. See text.
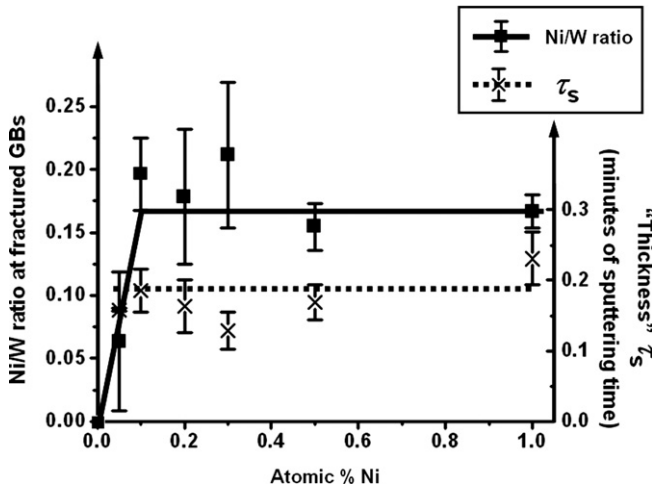
Fig. 7. Ni/W ratio at fractured GBs and fitted τ_s versus Ni content for specimens isothermally sintered at 1400 °C for 2 h. Error bars represent standard deviations.

The measured Ni/W ratio at the fractured GBs and fitted τ_s for the first set of specimens (0.05–1.0 at.% Ni, all sintered at 1400 °C for 2 h) are shown in Fig. 7. The Ni/W ratio is almost constant ($\sim$0.18) for specimens containing $\geqslant$0.1 at.% nickel, but is significantly lower for the specimen containing 0.05 at.% Ni ($\sim$0.06). The sputtering time (τ_s), which represents the relative thickness of the segregation layer, is virtually independent of the Ni content. These results suggest that equilibrium segregation has been achieved, because the segregation amount does not change with the increasing fraction of the secondary Ni phase.

For the second set of saturated specimens (1.0 at.% Ni) sintered at 1100–1475 °C, the measured Ni/W ratio at the fractured GBs is almost a constant (Fig. 8). The fitted sput-

tering time (τ_s), which represents the relative thickness of the segregation layer, decreases slightly with increasing temperature from 1100 °C to 1150 °C, and then increases with increasing temperature up to 1400 °C. At 1450 °C and 1475 °C, τ_s drops again. These results, although somewhat surprising, are consistent with the observed transitions in density and grain growth (Fig. 2b) as well as the occurrence of a triple-grain junction wetting transition (Fig. 5).

Fig. 9 shows HRTEM images of a representative GB in a W + 1 at.% Ni specimen sintered at 1400 °C (i.e. 95 °C below the bulk eutectic temperature). W lattice fringes are not contiguous at the GB and a $\sim$0.6 nm thick intergranular film is clearly identified. Despite indications of some local order existing within the film (Fig. 9d), the intergranular film is not fully crystallized. The digital image enhancement processes, including a background removal using fast Fourier transform (FFT) pass band filtering with a ($2 \, \text{nm}^{-1}$) aperture plus some brightness and contrast adjustments, have been used. These processes should not disturb any ordered or disordered features of <2 nm. Both unprocessed images (Fig. 9a and c) and processed images (Fig. 9b and d) are shown.

An ion milling effect has been observed; the Ni-enriched intergranular films are removed in the thinner region of specimens near the hole (Fig. 10). The same ion thinning effect has been previously reported for the ZnO–Bi$_2$O$_3$ system [24]. On the other hand, simultaneously imaging of a "clean" GB and a nanometer-thick intergranular film in one micrograph (Fig. 10) significantly reduces the problem of imaging artifacts (e.g. Fresnel fringes).

4. Discussion

4.1. Solid-state activated sintering mechanism

The observed enhanced densification and neck growth in W–Ni below the bulk eutectic temperature (Fig. 3b) reconfirms those reported in previous studies [1,2,5,8–11,17], but the sintered densities are slightly lower. High purity and the relatively large particle size of the powder used in this study are presumed to be responsible for the relatively low rates of densification. On the other hand, the use of pure materials (99.999+ %) in this study significantly reduces impurity effects on lowering the effective bulk eutectic temperature. Additionally, the W–Ni system exhibits a simple eutectic phase diagram where only two bulk phases (fcc (face-centered cubic) Ni and bcc (body-centered cubic) W) are present in the phase diagram in the temperature range 1060–1455 °C (Fig. 1) [40], excluding the possibility of forming a transient liquid phase. The pure nickel phase melts at 1455 °C (Fig. 1), i.e. 40 °C below the bulk eutectic temperature. Thus, the formation of a transition liquid cannot be completely excluded near and above 1455 °C, which may be related to significant grain growth (Fig. 8) or even the triple-grain junction wetting transition at 1450 °C (Fig. 5, considering the controlled temperature
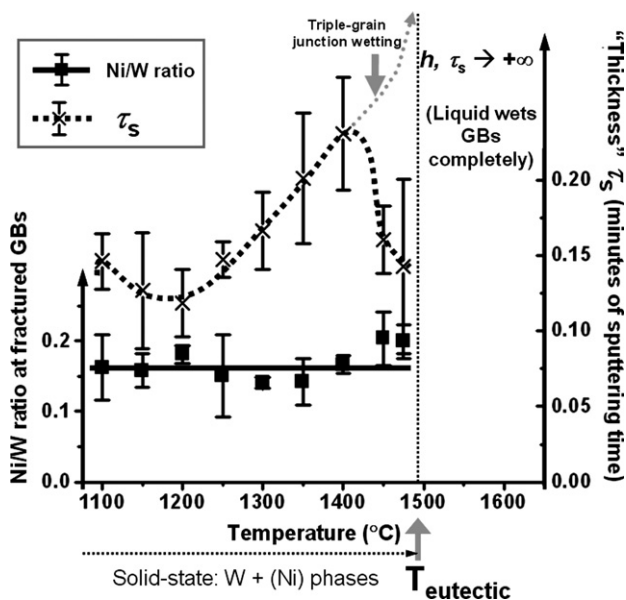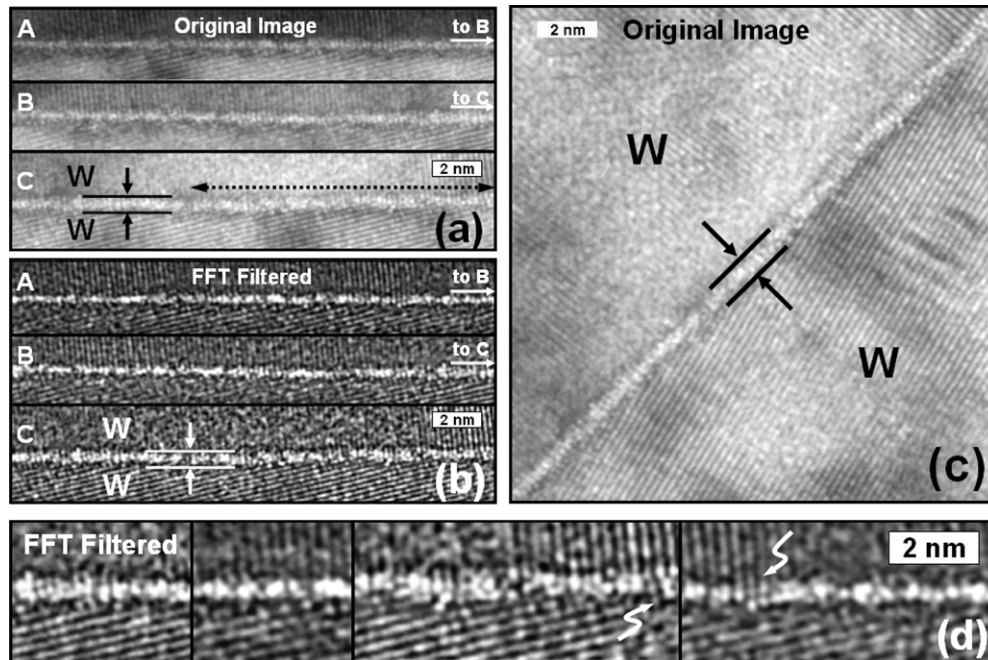

Fig. 8. Ni/W ratio at fractured GBs and fitted τ_s versus sintering temperature. All specimens contain 1.0 at.% Ni and were sintered isothermally for 2 h. Error bars represent standard deviations.

Fig. 9. (a) Original and (b) digitally enhanced HRTEM images of a ~0.6-nm thick, disordered, GB film in a W + 1 at.% Ni specimen sintered at 1400 °C. The film thickness is nearly constant along the GB. (c) Original HRTEM image of a selected segment of the long film shown in (a) (which is indicated by the dotted arrow in (a)), where the image is magnified and rotated 45°. (d) Images of selected areas in (b) on an expanded scale. The digital enhancement process includes a background removal using FFT pass band filtering with a (2 nm^{-1}) aperture plus some brightness and contrast adjustments, which should not disturb any features <2 nm.
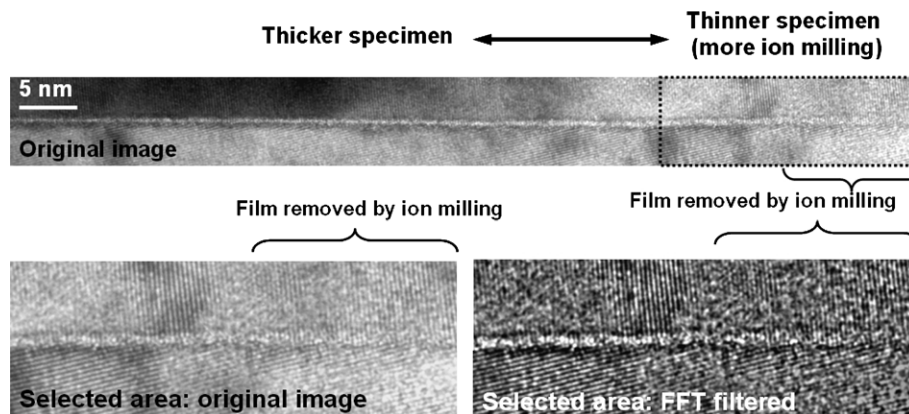

Fig. 10. The film was removed in the thinner section of specimen (that is closer to the hole). The same ion milling effect was reported previously for intergranular films in Bi$_2$O$_3$-doped ZnO [24].

precision and uniformity are ~5 °C for the tube furnace used in the experiments). Nonetheless, this study unequivocally illustrates the nickel activated sintering of tungsten without the presence of any stable or transient bulk liquid phases for specimens sintered between 1100 °C and 1400 °C.

This study demonstrates that the Ni-rich, crystalline, secondary phase is not the solid-state activator as was previously suggested [1,4]. Fig. 4 clearly illustrates that the Ni-rich secondary bulk phase does not completely wet and penetrate along the GBs. The fact that the crystalline Ni phase does not even wet the triple-grain junctions at 1400 °C (Fig. 5a) indicates that the dihedral angle is >60°, which is consistent with the direct observation in Fig. 4. The Ni-rich crystalline secondary phase is present at four-grain junctions as isolated particles (Fig. 4) at and below 1400 °C when activated sintering is significant. Consequently, they cannot be an effective activator to facilitate densification in the solid state. It is therefore concluded that the solid-state activator should be an interfacial segregation layer or a nanoscale interfacial phase. This conclusion is directly supported by the Auger depth profiling results (Fig. 6), which show that the equivalent thickness of nickel segregation layer is on the order of 1 nm.

HRTEM showed that nanometer-thick disordered films form at GBs well below the bulk eutectic temperature (Fig. 9). These nanoscale interfacial films are likely to satisfy all prerequisites for being an effective activator. They segregate at GBs and likely have significant solubility for the base material (since the GB films are a quasi-liquid phase and the bulk eutectic liquid contains 20.7 at.% W [40]). Furthermore, it is reasonably expected that such quasi-liquid films exhibit high excess free volume and can provide a short-circuit diffusion path for the base material. Consequently, the solid-state activated sintering in nickel-doped tungsten can be attributed to enhanced mass transport in these sub-solidus disordered interfacial films.

The proposed sintering mechanism is also consistent with the observed densification versus nickel content (Fig. 2a), in which the densification rate remains steady for specimens containing more than ∼0.3% nickel. This demonstrates that excess nickel addition beyond what is needed to form nanometer-thick interfacial films does not provide additional benefits for sintering. It is not surprising that the optimal doping level for activated sintering is slightly greater than the solid solubility (∼0.2% Ni at 1400 °C [40]) because the formation of equilibrium interfacial films requires the nickel to transport into the GB region. Similar densification versus nickel content has been widely observed in previous studies [4,9,10] and is considered a universal characteristic of solid-state activated sintering of refractory metals.

It is generally believed that Langmuir–McLean or truncated BET type GB adsorption in metals will hinder GB diffusion [41,42]. This argument is based on a rather intuitive premise: adsorbates fill the open adsorption sites and reduce the excess free volume at GBs, thereby reducing the GB diffusivity. However, this study suggests an opposite trend at high temperatures: interfacial adsorption can induce GB disordering near the bulk eutectic or solidus temperatures, thereby creating more excess free volume and enhancing GB diffusion.

4.2. Stabilization of sub-eutectic disordered intergranular films

It is imperative to discuss further the character and formation mechanism of these newly observed disordered intergranular films in Ni-doped W. These Ni-enriched intergranular films are likely to have become more ordered during cooling. The fact that these intergranular films appear to be largely disordered in cooled specimens implies that the high temperature GB cores must be even more disordered and perhaps wider. On the other hand, the high triple-grain junction wetting temperature (Fig. 5) in Ni-doped W provided a unique experimental opportunity. For specimens annealed at 1400 °C, the secondary Ni-rich phase is present as isolated particles (Fig. 5a). Without the continuous presence of a secondary phase at triple-grain junctions as nuclei, it is difficult for Ni to diffuse out or fully crystallize upon cooling; thus the GB chemistry and structure are

better preserved. Furthermore, these disordered intergranular films are not a result of solid-state amorphization [43] because no intermediate compound is present in the phase diagram at 1400 °C (Fig. 1) [40].

Presumably, the formation of crystalline intergranular phase is frustrated by high interfacial energies to create two crystal-to-crystal hetero-phase interfaces. The stabilization of a sub-eutectic, quasi-liquid film can be conceived as if the increased free energy for forming the under-cooled liquid film is over-compensated by the reduction in interfacial energies upon replacing a high-energy GB with two low-energy crystal–liquid interfaces (Fig. 11):

$$\Delta G_{\text{amorph.}} \cdot h < \gamma_{\text{gb}}^{(\text{W})} - 2\gamma_{\text{cl}} \equiv \Delta \gamma \qquad (2)$$

where h is the film thickness, $\gamma_{\text{gb}}^{(\text{W})}$ and γ_{cl} are the excess free energy for the W GB and the crystal–liquid interface, respectively, and $\Delta G_{\text{amorph.}}$ is the volumetric amorphization energy for forming under-cooled liquid below the bulk eutectic temperature.

In this case, $\Delta G_{\text{amorph.}}$ should be positive. First, since the Ni concentration in the W particles was zero before sintering (with Ni being added as a secondary phase), the Ni concentration in the W grains after the sub-eutectic isothermal sintering should be equal to the bulk solid solubility limit (if a chemical equilibrium has been achieved) or possibly be below it (if an equilibrium has not been achieved). In either case, $\Delta G_{\text{amorph.}}$ is positive (see further elaboration in Section 4.3). Second, the specimens have never been heated above the bulk eutectic/solidus temperatures; thus, it is unlikely that a bulk liquid phase has formed and been retained in the specimens (excluding a possible reason for zero $\Delta G_{\text{amorph.}}$). Finally, there are no intermediate compounds in the W–Ni binary phase diagram (Fig. 1) between 1060 °C and 1495 °C (one of the reasons that we selected this model system in the first place), thus excluding the possibility of forming a "transient liquid" or the occurrence of solid-state amorphization (which are the other possible reasons for negative $\Delta G_{\text{amorph.}}$).

If these disordered intergranular films form from mixing and amorphizing the two equilibrium bulk crystalline phases W(Ni) and Ni(W), $\Delta G_{\text{amorph.}}$ is zero at the eutectic temperature and can be estimated using the first derivative at finite undercooling:

$$\Delta G_{\text{amorph.}} \approx \Delta S_{\text{amorph.}} \cdot (T_{\text{eutectic}} - T) \qquad (3)$$
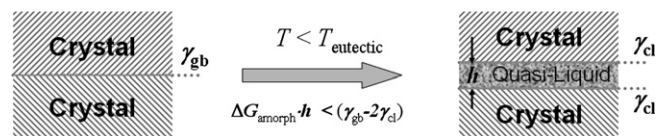
where we define:

Fig. 11. Below the bulk eutectic temperature, a thin quasi-liquid layer can be stabilized at grain boundaries if the increased free energy for forming the undercooled liquid layer is over-compensated by the reduction in the total interfacial energies.

$$\Delta S_{\text{amorph.}} \equiv \frac{\mathrm{d}(\Delta G_{\text{amorph.}})}{\mathrm{d}T}\bigg|_{T=T_{\text{eutectic}}} \tag{4}$$

A previous experiment showed that the nickel-rich liquid completely wets the tungsten GBs slightly above the bulk eutectic temperature [44]. Thus, $\Delta\gamma$ should be greater than zero and the stabilization of a sub-eutectic liquid film can be thermodynamically rationalized for an undercooling range of:

$$0 < (T_{\text{eutectic}} - T) \leqslant \frac{\Delta\gamma}{h \cdot \Delta S_{\text{amorph.}}} \tag{5}$$

Furthermore, tungsten exhibits a high GB energy ($\gamma_{\text{gb}}^{(W)} > 1$ J m^{-2} at 1500 °C [45]), implying quasi-liquid films can be stabilized at GBs over a significant range of undercooling. A rough estimation using a one-component equation showed that the stabilization of a 0.6-nm thick Ni liquid film at an undercooling of 95 °C only requires a reduction of 10% in the tungsten GB energy [39].

4.3. Related interfacial phenomena

Several well-known interfacial phenomena, namely equilibrium-thickness intergranular films in ceramics [19,23,24,46–51], premelting [29–32], prewetting [33] and multilayer adsorption [52–54], have features in common with the present case. The basic observations of nanoscale intergranular and surficial films have been recently reviewed [51,55–58], among which a critical assessment article [58] reviews and compares related nanoscale interfacial phenomena of premelting, premelting, frustrated-complete wetting, intergranular and surficial amorphous films in ceramics, and their metallic counterparts, with the goal of establishing a unified thermodynamic framework. Critical assessments of the present observations with respect to other well-known interfacial phenomena and theories are made in the following text.

The observed GB films in Ni-doped W can be considered as metallic counterparts to equilibrium-thickness intergranular films (IGFs) that have been widely observed in Si$_3$N$_4$ and other ceramic materials [19,23,24,46–51]. These IGFs can alternatively be understood to be quasi-liquid layers which adopt an "equilibrium thickness" in response to a balance among several specific interfacial interactions that individually may act to thin or thicken the film [46,47] or multilayer adsorbates with compositions and GB excesses set by the bulk chemical potentials [48,59]. We expect that the disordered GB films in this binary metallic system may follow a relatively simple combined GB prewetting and premelting diffuse-interface model [60]. On the other hand, IGFs in ceramics are in principle more complex (because there are more interfacial forces, e.g. electrostatic interactions, and a metastable equilibration is more likely), thereby resulting in more complicated and diversifying interfacial behaviors. Some differences between ceramic IGFs and their metallic counterparts are expected. For example, the film thickness may be divergent

(approaching infinity) at the bulk eutectic temperature in Ni-doped W, since a complete GB wetting transition has been observed slightly above the bulk eutectic temperature [44]. For ceramic materials, however, nanometer-thick IGFs in general persist into the solid–liquid coexistence regime, where the presence of an attractive dispersion interaction of significant strength is presumed to restrain the unlimited thickening of the film. Additionally, disordered films in non-glass-forming metallic systems are more likely to order/crystallize during cooling. These are possible reasons why such disordered intergranular films have not been widely found in metals.

The stabilization of sub-eutectic disordered GB films is phenomenologically analogous to the theory of surface melting or premelting [29–32], which refers to the formation of a thin, surface, quasi-liquid layer below the bulk melting temperature in one-component systems. Convincing experimental evidence for surface premelting has been obtained for ice [30,31] and lead [61]. Driven by the reduction of the interfacial energies, a quasi-liquid layer may also be stabilized at GBs below the bulk melting temperature, known as GB premelting. In 1989, Hsieh and Balluffi reported [62] an in situ hot-stage TEM experiment which concluded that GB premelting is likely to occur for pure Al, but only above $0.999 T_{\text{melting}}$. Subsequently, exploration in this area was greatly discouraged. The occurrence of GB disordering transitions in Si [63,64] and fcc metals [65,66] has also been suggested from molecular dynamics simulations. Nonetheless, the extent to which GB premelting occurs in one-component materials remains controversial.

If these nanoscale intergranular films in Ni-doped W indeed formed in a thermodynamic equilibrium with the two equilibrium bulk crystalline phases (which is likely according to the discussions in Section 4.2 and the next paragraph), they can be considered as "segregation-induced GB premelting" in two-component materials. In principle, such disordered GB structures can occur over a wider range of undercooling than the simple premelting in one-component materials because GB disordering can be enhanced by a concurrent segregation/adsorption. Herein, a model should be developed from a generalization of Cahn's critical point wetting theory [33]. Prewetting and critical point wetting theories [33] were initially proposed for binary liquid systems exhibiting immiscibility and have been confirmed for organic systems [67] and Pb–Ga liquid metal [68]. The observed Ni-enriched disordered films at tungsten GBs can be understood as a class of combined GB disordering and adsorption structures resulting from coupled GB premelting and prewetting transitions, where a recently proposed diffuse-interface model [60] should be applicable. Researchers also indirectly revealed possible GB premelting/prewetting transitions in Bi-doped Cu [18,69] and (Si, Zn)-doped Fe [18,70,71] by measuring GB diffusivities and chemistry, which may correspond to similar disordered GB structures.

According to conventional definitions, these nanoscale intergranular films in Ni-doped W can be considered in

the prewetting/premelting regime if the bulk liquid phase is thermodynamically unstable or $\Delta G_{amorph.}$ in Eq. (2) is positive. Assuming the chemical potentials of the intergranular films are at least in a local equilibrium with the adjacent W grains, the above conditions require that the Ni concentration in W grains (which is different from the nominal overall composition) is lower than the metastable extension of the solidus line (i.e. the concentration of metstable W(Ni) alloy which is in equilibrium with the under-cooled liquid phase). In the present case, the initial powders consist of mechanically mixed pure W particles and Ni addition as a secondary phase. During the isothermal sintering (in a regime where only the W(Ni) and Ni(W) phases are stable), some Ni must have been dissolved into the W grains/phase, but it is unlikely that the Ni concentration in W grains could go above the bulk solid solubility limit of Ni in W (which is lower than the metastable extension of the solidus line). Furthermore, additional Ni dopants beyond the bulk solid solubility limit resulted in no further benefits for densification (Fig. 2a) and no significant difference in Ni segregation at W GBs (Fig. 7). Hence, it is likely that a chemical equilibrium has been achieved between the W(Ni) and Ni(W) bulk phases and the intergranular films. Although EDX and Auger analyses do not have sufficient accuracy to determine the Ni concentration in the W grains quantitatively (which should be approximately 0.2 at.% at 1400 °C [40]), EDX analysis showed that the W concentration in the Ni-rich secondary phase is close to the equilibrium value (Fig. 4).

If these disordered intergranular films were in a local equilibrium with oversaturated W grains containing Ni concentrations that are higher than the metastable extension of the solidus line, they might still exhibit an equilibrium thickness as a result of a balance between several attractive and repulsive interfacial forces. Equilibrium-thickness IGFs in some ceramic materials may represent similar situations. It is worthy noting that IGFs in ceramics have also been observed to form under sub-solidus and sub-eutectic conditions [24,72,73], where they may also be considered in the prewetting/premelting regime with additional interfacial interactions (e.g. dispersion and electrostatic forces) that tune the film thickness.

Furthermore, one may interpret the Ni-enriched, nanoscale interfacial films as multiple adsorbed layers at GBs from the viewpoint of adsorption. Gibbs adsorption theory should apply. Inspired by Kikuchi and Cahn's lattice-gas model [74], Cannon recently suggested [59] the existence of two distinct regions of GB adsorption: a well-known Langmuir/BET segregation region that occurring at relatively low-temperatures, which is characterized by a fixed number of adsorption sites; and an interfacial prewetting/ premelting behavior occurring close to the bulk solidus or eutectic temperatures, where GB adsorption promotes GB disordering and creates new adsorption sites. These two regions are characterized by the opposite temperature-dependence on GB excess. As shown in Fig. 8, the segregation amount decreases slightly with increasing temperature initially (1100–1200 °C); this appears to be consistent with classical segregation models where a thermally activated desorption is expected with increasing temperature, but the effect is too small to draw a conclusion. Above 1200 °C, the equivalent thickness of the segregation layer appears to increase with increasing temperature, suggesting the occurrence of GB prewetting/premelting at higher temperatures, where the adsorption causes GB disordering and creates additional adsorption sites. Ni/W ratio at the GB core is almost independent of temperature (Fig. 8), implying that the additional disordering/adsorption mainly occurs in the consecutive layers, i.e. the formation of a multilayer disordered GB core. Above 1450 °C, the GB excess drops again, occurring coincidentally with the occurrence of triple-grain junction wetting (Fig. 5) and rapid grain growth (Fig. 2b), which is likely to be an artifact caused by the increasing difficulty in preserving GB chemistry during cooling (with continuous nucleation sites at triple-grain junctions) as well as the moving boundary effects. Since a complete GB wetting was evident at 1550 °C [44], it is reasonably expected that the film thickness is divergent at the bulk eutectic temperature (Fig. 8). However, in principle an attractive dispersion force still exist and the GB wetting transition can be first order (meaning a discrete jump of film thickness from a finite value to infinity). Further research using well-quenched specimens or hot-stage TEM is in progress.

4.4. Other properties and systems

In a previous study [75], a minor addition of Ni was found to promote rapid grain growth, which somewhat contrasts with the classical theory of solute-drag to GB migration. The rapid GB migration was also evident in this study from the significant pore-boundary and precipitate-boundary separations (Fig. 3c and d). Close to the bulk eutectic temperature, the GB mobility increases dramatically, resulting in significant grain growth and a reduction in the final sintered density (Fig. 2b) owing to the trap of pores inside the grains (Fig. 3c). This study implies a non-classical type of solute effect on GB migration, i.e. segregation enhances GB mobility by promoting GB disordering. Rapid GB migration associated with the formation of prewetted or disordered GB films has been confirmed for ceramic systems $(Y_2O_3 + SiO_2)$-doped Al_2O_3 [72] and Bi_2O_3-doped ZnO [76], and suggested for Ga-doped Al [69]. This new mechanism should compete with the solute-drag effect; significant grain growth (Fig. 2b) can occur if it overwhelms the solute-drag effect. A competition between prewetting and the solute-drag effects to GB mobility has been quantitatively assessed using Al–Ga as a model system [77]. It should be noted that diffusion-induced grain boundary migration [78,79] may be another reason for the observed rapid GB migration.

Similar solid-state activated sintering behaviors have been demonstrated for a broad range of doped refractory metals, e.g. W–Pt, W–Pd, W–Fe, W–Co and Mo–Ni

(where the primary phases are underlined) [1–15,17,18]. In general, densification of refractory metals is strongly enhanced with minor addition of a transition metal, typically at level of about 1-nm thick coatings on the original powder. Enhancement of solid-state GB diffusion must relate to some degree of GB adsorption and disorder, but exactly what controls this behavior is not obvious. It is unknown whether nanometer-thick disordered GB films form in all of these refractory metal systems. A recent study identified an approximately 2-nm thick crystalline δ-NiMo compound layer at GBs in Ni-doped Mo specimens that were sintered in the solid state and quenched [15]. As a key difference between W–Ni and Mo–Ni, δ-NiMo is an equilibrium bulk compound phase at the typical activated sintering temperatures for Ni-doped Mo. It is unknown whether such intergranular layers in Ni-doped Mo are disordered at the sintering temperature and whether they exhibit an "equilibrium thickness." Further investigations are needed to revisit the activated sintering mechanism of these refractory metals.

Additionally, activated sintering of refractory metals constantly results in significant GB embrittlement, which may also relate to the unrecognized existence of such GB layers. Finally, the presence of quasi-liquid GB films should also have a critical impact on a range of other GB related properties, e.g. creep, corrosion and oxidation resistance, at high processing or operating temperatures, or at the room temperature if GB structure and chemistry are partially preserved upon cooling.

5. Conclusions

Experiments using high purity W–Ni material as a model two-component refractory metal system unequivocally confirmed the occurrence of solid-state activated sintering. Densification, grain growth and GB chemistry were measured as a function of sintering temperature and nickel content. The Ni-rich secondary bulk phase does not wet and penetrate along GBs; furthermore, it does not wet tungsten triple-grain junctions until ∼50 °C below the bulk eutectic temperature. Thus, the Ni-rich bulk phase cannot be an effective solid-state activator for facilitating sub-eutectic densification. HRTEM and AES revealed the stabilization of nanometer-thick, nickel-enriched, disordered films at GBs well below the bulk eutectic temperature. Consequently, solid-state activated sintering is attributed to enhanced mass transport in these disordered interfacial films.

These disordered GB films in W–Ni can be regarded as metallic counterparts to the widely observed equilibrium-thickness intergranular films or IGFs in ceramics. This new observation is scientifically significant because these metallic IGFs can be used to validate a relatively simple model, which can then serve as a basis for developing a more complex model for IGFs in ceramics by adding extra interfacial forces, e.g. electrostatic forces. This study, along with several earlier studies of solid-state activated sintering

in ceramic materials, demonstrated that bulk phase diagrams are not always accurate for predicting the stability of nanoscale quasi-liquid interfacial films and the occurrence of activated sintering.

References

[1] Brophy JH, Shepard LA, Wulff J. The nickel-activated sintering of tungsten. In: Leszynski W, editor. Powder metallurgy. Interscience; 1961. p. 113.
[2] Hayden HW, Brophy JH. J Electrochem Soc 1963;110:805.
[3] Prill AP, Hayden WW, Brophy JH. Trans AIME 1964;230:769.
[4] Toth IJ, Lockington NA. J Less-Common Met 1967;12:353.
[5] Flether G, James MR, Moon JR. Scripta Met 1971;5:105.
[6] German RM, Munir ZM. Metall Trans A 1976;7A:1873.
[7] Coble RL, Cannon RM. Current paradigms in powder processing. In: Palmour HI, editor. Processing of crystalline ceramics. New York: Plenum Press; 1978. p. 151.
[8] Lee DN, Ahn SH. Sci Sinter 1979;11:43.
[9] German RM. Rev Powder Metall Phys Ceram 1982;2:9.
[10] German RM. Prog Powder Met 1984;39:243.
[11] Yoon H, Kim J-S, Kim Y-L. J Less-Common Met 1984;102:219.
[12] German RM. Mod Dev Powder Met 1985;15:253.
[13] Johnson JL, German RM. Metall Mater Trans 1996;27A:441.
[14] Hwang NW, Park YJ, Kim D-Y, Yoon DY. Script Mater 2000;42:421.
[15] Hwang KS, Huang HS. Acta Mater 2003;51:3915.
[16] Kingery WD. J Appl Phys 1959;30:301.
[17] Panichkina VV et al. Sov Powder Metall Phys Ceram 1967;6:558.
[18] Straumal BB, Noskovich OI, Semenov VN, Shvindlerman LS, Gust W, Predel B. Acta Metall Mater 1992;40:795.
[19] Luo J, Wang H, Chiang Y-M. J Am Ceram Soc 1999;82:916.
[20] Li G. Sci Sinter 1987;19:167.
[21] Skaar EC. Activated sintering in calcium fluoride, sodium fluoride system. Ph.D. thesis, M.I.T., Cambridge, MA; 1977.
[22] Duvigneaud PH, Reinhard D. Sci Ceram 1984;12:287.
[23] Chiang Y-M, Wang H, Lee J-R. J Microsc 1998;191:275.
[24] Wang H, Chiang Y-M. J Am Ceram Soc 1998;81:89.
[25] Luo J, Chiang Y-M. J Eur Ceram Soc 1999;19:697.
[26] Luo J, Chiang Y-M. Acta Mater 2000;48:4501.

[27] Luo J, Tang M, Cannon RM, Carter WC, Chiang Y-M. Mater Sci Eng A 2006;422:19.

[28] Luo J, Chiang Y-M, Cannon RM. Langmuir 2005;21:7358.

[29] Dash JG. Contemp Phys 1989;30:89.

[30] Dash JG, Fu H, Wettlaufer JS. Rep Prog Phys 1995;58:115.

[31] Dash JG, Rempel AM, Wettlaufer JS. Rev Mod Phys 2006;78: 695.

[32] van der Veen JF, Pluis B, Denier AW. Surface melting. In: Vanselow R, Howe RF, editors. Chemistry and physics of solid surfaces, vol. 7. Berlin: Springer; 1988. p. 455.

[33] Cahn JW. J Chem Phys 1977;66:3667.

[34] Jud E, Zhang Z, Sigle W, Gauckler LJ. J Electroceram 2006;16:191.

[35] Jud E, Huwiler CB, Gauckler LJ. J Am Chem Soc 2005;88:3013.

[36] Nieh TG. Scripta Met 1984;18:1279.

[37] Kim S-W, Lee S-I, Kim YD, Moon I-H. Int J Refract Met Hard Mater 2003;21:183.

[38] Lee JS, Klockgeter K, Herzig C. Coll Phys 1990;51:C1.

[39] Luo J, Gupta VK, Yoon DH, Meyer III HM. Appl Phys Lett 2005;87:231902.

[40] Massalski TB, Okamoto H. Binary alloy phase diagrams. Materials Park (OH): ASM International; 1990.

[41] Gottstein G, Molodov DA. Interf Sci 1998;6:7.

[42] Lejcek P, Hofmann S. Crit Rev Solid State Mater Sci 1995;20:1.

[43] Johnson WL. Materials interfaces. New York: Chapman and Hall; 1992. p. 517.

[44] Liu Y, Iacocca RG, Johnson JL, German RM, Kohara S. Metall Mater Trans A 1993;26A:2484.

[45] Hodkin EN, Nicholas MG, Poole DM. J Less-Common Met 1970;20:93.

[46] Clarke DR. J Am Ceram Soc 1987;70:15.

[47] Clarke DR, Shaw TM, Philipse AP, Horn RG. J Am Ceram Soc 1993;76:1201.

[48] Cannon RM, Esposito L. Z Metallkd 1999;90:1002.

[49] Kleebe H-J. J Ceram Soc Jpn 1997;105:453.

[50] Kleebe H-J, Cinibulk MK, Cannon RM, Rühle M. J Am Ceram Soc 1993;76:1969.

[51] Subramaniam A, Koch CT, Cannon RM, Rühle M. Mater Sci Eng A 2006;422:3.

[52] Pandit R, Schick M, Wortis M. Phys Rev B 1982;26:5112.

[53] Chiang Y-M, Henriksen AF, Kingery WD, Finello D. J Am Ceram Soc 1981:64.

[54] Chang LS, Rabkin E, Straumal BB, Baretzky B, Gust W. Acta Mater 1999;47:4041.

[55] Luo J, Qian H, Shi X. Interface stabilized nanometer-thick disordered films. In: Nalwa HS, editor. Encyclopedia of nanoscience and nano-technology, 2nd ed. Velencia, CA: American Scientific Publishers [in press].

[56] Luo J. Stabilization of nanometer-thick quasi-liquid interfacial films: from ceramics to metals and beyond. In: Cook LP, Kaplan WD, editors. Materials science and technology 2006: fundamentals and characterization, vol. 2. Cincinnati, OH; 2006. p. 239.

[57] Luo J, Chiang Y-M, Cannon RM. Inorganic nanoscale surficial films of self-selecting thickness. In: Nalwa HS, Ariga K, editors. Bottom-up nanofabrication: superamolecules, self-assemblies and organized films. Valencia, CA: American Scientific Publishers [in press].

[58] Luo J. Critical reviews in solid state and materials sciences (submitted for publication).

[59] Cannon RM. Unpublished results; 2006.

[60] Tang M, Carter WC, Cannon RM. Phys Rev Lett 2006;97:075502.

[61] Frenken JWM, Maree PM, van der Veen JF. Phys Rev B 1986;34:7506.

[62] Hsieh TE, Balluffi RW. Acta Metall 1989;37:1637.

[63] Keblinski P, Phillpot SR, Wolf D. Phys Rev Lett 1996;77:2965.

[64] Keblinski P, Phillpot SR, Wolf D, Gleiter H. J Am Ceram Soc 1997;80 717.

[65] Wolf D. Curr Opin Solid State Mater Sci 2001;5:435.

[66] Keblinski P, Wolf D, Phillpot SR, Gleiter H. Philos Mag A 1999;79:2735.

[67] Kellay H, Bonn D, Meunier J. Phys Rev Lett 1993;71:2607.

[68] Wynblatt P, Chatain D. Ber Bunsen Phys Chem 1998;102:1142.

[69] Straumal BB, Baretzky B. Interf Sci 2004;12:147.

[70] Noskovich OI, Rabkin EI, Semenov VN, Straumal BB, Shvindlerman LS. Acta Metall Mater 1991;39:3091.

[71] Rabkin EI, Semenov VN, Shvindlerman LS, Straumal BB. Acta Metall Mater 1991;39:627.

[72] MacLaren I, Cannon RM, Gülgün MA, Voytovych R, Pogrion NP, Scheu C, et al. J Am Ceram Soc 2003;86:650.

[73] Ackler HD, Chiang Y-M. J Am Ceram Soc 1997;80:1893.

[74] Kikuchi R, Cahn JW. Phys Rev 1987;B36:418.

[75] Moon I-H, Kim K-Y, Oh S-T, Suk M-J. J Alloys Compd 1993;201:129.

[76] Choi JH, Hwang N-M, Kim DY. J Am Ceram Soc 2001;84:1398.

[77] Weygand D, Breichet Y, Rabkin E, Straumal B, Gust W. Philos Mag Lett 1997;76:133.

[78] Rabkin E, Gust W, Fournelle RA. Interf Sci 1998;6:105.

[79] Hillert M. Acta Mater 1999;47:4481.